Simple and Efficient Numerical Evaluation of Near-Hypersingular Integrals

Patrick W. Fink[(1)*], Donald R. Wilton[(2)], Michael A. Khayat[(1)]

(1) NASA Johnson Space Center, Houston, Texas, Electromagnetic Systems Branch
(2) University of Houston, Texas, Department of Electrical and Computer Engineering

Introduction

Recently, significant progress has been made in the handling of singular and nearly-singular potential integrals that commonly arise in the Boundary Element Method (BEM) [1-3]. To facilitate object-oriented programming and handling of higher order basis functions, cancellation techniques are favored over techniques involving singularity subtraction. However, gradients of the Newton-type potentials, which produce hypersingular kernels, are also frequently required in BEM formulations. As is the case with the potentials, treatment of the near-hypersingular integrals has proven more challenging than treating the limiting case in which the observation point approaches the surface. Historically, numerical evaluation of these near-hypersingularities has often involved a two-step procedure: a singularity subtraction to reduce the order of the singularity, followed by a boundary contour integral evaluation of the extracted part. Since this evaluation necessarily links basis function, Green's function, and the integration domain (element shape), the approach ill fits object-oriented programming concepts. Thus, there is a need for cancellation-type techniques for efficient numerical evaluation of the gradient of the potential.

Progress in the development of efficient cancellation-type procedures for the gradient potentials was recently presented [2, 4]. To the extent possible, a change of variables is chosen such that the Jacobian of the transformation cancels the singularity. However, since the gradient kernel involves singularities of different orders, we also require that the transformation leaves remaining terms that are analytic. The terms "normal" and "tangential" are used herein with reference to the source element. Also, since computational formulations often involve the numerical evaluation of both potentials and their gradients, it is highly desirable that a single integration procedure efficiently handles both.

Transformation and Method for Near-Hypersingularities

In order to simplify the presentation and evaluation of the proposed methods, we consider the following integral representative of the actual integrals with respect to the convergence of numerical integration:

$$I = \int_{\mathcal{D}} b(r') \nabla \left(\frac{e^{-jkR}}{4\pi R} \right) d\mathcal{D} \,, \tag{1}$$

where $R = |\mathbf{r} - \mathbf{r}'|$ is the distance between an observation point at $\mathbf{r}$ and source points on triangular domains $\mathcal{D}$. Here, the function b is intended to capture the functional content of the basis function in scalar form. Following previous approaches [1-5], a nearby observation point is projected onto the surface containing the source parent triangular element. The parent triangle is then split into three subtriangles about the projected observation point. The geometry of a typical subtriangle and its local rectangular coordinate system with origin at the projected observation point is shown in Fig. 1(a). The general form of the transformed integral over the subtriangle is given by

$$\int_0^h \int_{y\cot\phi_L}^{y\cot\phi_U} g(x,y)\mathbf{R}\, dxdy = \int_{u_L}^{u_U} \int_{v_L}^{v_U} g\left[x(u,v), y(u,v)\right] \mathcal{J}(u,v)\, \mathbf{R}\, dvdu\,, \tag{2}$$

where $g(x, y)$ is a product of the basis and the Green's function. In determining a suitable transformation, care must be exercised so as not to introduce non-analytic or nearly singular functions. A transformation previously investigated [2, 4] can be summarized as $v = \ln R$ and $u = \ln\left[\tan(\phi/2)\right]$. Terms involving odd powers of ρ, which are non-analytic in v, must be handled carefully. In addition, this so-called R^2 transformation can result in slow convergence when the difference between limits, $v_U - v_L$, is large.

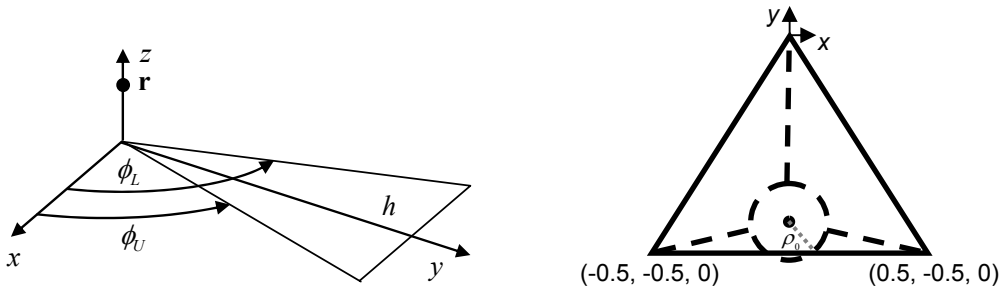

Fig. 1 – (a) Subtriangle coordinates and assigned parameters. (b) Subtriangle and disk elements.

To address these difficulties with the R^2 transformation, we introduce a disk of radius ρ_0 centered at the projection point as shown in Fig. 1(b), along with three truncated subtriangles. The introduction of this fourth sub-element provides three important advantages. First, the azimuthal variation of the gradient can be integrated exactly using only two equi-spaced sample points for constant basis functions or with three equi-spaced sample points for linear basis functions (completeness order p = 0). The second advantage arises from the elimination of the non-analytic terms, ρ, over the disk. Thirdly, as we now show, the remaining radial variation of the integrand can be accurately and efficiently integrated. Assuming a basis function of linear order, and application of the radial transformation, $R = \ln v$, the inner integral over the disk element can be written

$$\mathbf{I}_{disk}^{R} = \int_{v_l}^{v_u} \left(jk + R^{-1}\right) e^{-jkR} \left[\left(R^2 - z^2\right)\mathrm{cir}_x^2(\phi), \left(R^2 - z^2\right)\mathrm{cir}_y^2(\phi), \kappa z\right] dv\,, \tag{3}$$

where the functions $\mathrm{cir}^2(\phi)$ represent sums of second order terms of the form $\sin^2(\phi)$, $\cos^2(\phi)$, and $\sin(\phi)\cos(\phi)$, and the dependency of R on v has been suppressed for notational simplicity. We assume that the source element is sufficiently small that the phase term can be expressed accurately as a Taylor series truncated to only a few terms, and employ a quadrature rule to numerically integrate the resulting exponential terms. We obtain such a rule by solving the system of equations

$$\sum_{k=1}^{(m_{\max}+2)/2} w_k \, e^{m\beta\lambda_k} = \int_0^1 e^{m\beta\lambda} d\lambda \,, \quad m = -1, 0, 1, ..., m_{\max} \,, \tag{4}$$

in which $\beta \equiv \ln(R_0/z)$. We can precompute a table of quadrature rules to cover the desired range of $\delta \equiv \rho_0/z$. To use the tables, we choose the nearest tabulated entry $\tilde{\delta} \equiv \tilde{\rho}_0/z$, then modify the disk radius $\rho_0 \to \tilde{\rho}_0$ and corresponding parameter, $\tilde{R}_0$, to match the selected table entry. Orders through $m_{\max}$ are integrated exactly over the disk, and the insensitivity of the method to the radius, $\tilde{\rho}_0$, is demonstrated in the next section. A table accommodating values $0.5 < \tilde{\delta} < 10^5$ and disk radius increments of twenty percent can be achieved with a table of approximately 70 quadrature rules. We treat the remaining truncated subtriangles using the transformations $v = \ln R$ and $u = \ln\left[\tan(\phi/2)\right]$.

Numerical Results

The method described above is tested with the source element shown in Fig. 1(b) and for observation points at (0, -0.4, *z*) meters, where *z* is varied for three cases, 10^{-6}, 0.01, and 0.2 m. The basis function variation is chosen as $b = x + y$ (Fig. 1(b)), and the disk radius is set to 0.1 m (except for one case that demonstrates insensitivity to this parameter). For reference solutions, *x*-*y* integration over the triangle of Fig. 1(b) is achieved with a discretization cell size that increases with increasing distance from the projection point; i.e., an *h*-refinement. For efficient integration of the exponential terms over the disk, we choose $m_{\max} = 2$, which entails a 2-point quadrature rule. Each truncated subtriangle was analyzed individually to determine near-optimal ratios for sampling in order to achieve a near monotonic convergence for both the normal and tangential gradient components. Convergence trends of the normal and tangential components are shown in Figs. 2(a) and 2(b), respectively, with the number of sample points indicating the combined total for the disk and all three subtriangle regions. As seen in Fig. 2(a), accurate integration of the normal gradient component is extremely efficient as *z* tends to zero. The crossed square symbols in this figure denote disk quadrature schemes with fewer than six sample points. The cross symbols in Fig. 2(a) represent use of a disk radius $\rho_0 = 0.09$, and it can be seen that the effects of adjusting the disk radius are minimal. Fig. 2(b) also shows the convergence results for the potential using the same quadrature rules developed for the gradient. Clearly, the same rule can be used for both.

Conclusion

A technique for efficient numerical evaluation of hypersingular kernels is demonstrated. It is also shown that weaker singularities may be handled efficiently by the same technique. As the projection of the observation point approaches an edge of the source element, the efficiency of the technique is reduced. Treatment of this case remains as future work. Additional work also includes extending the technique to handle projections of the observation point falling outside the source element.

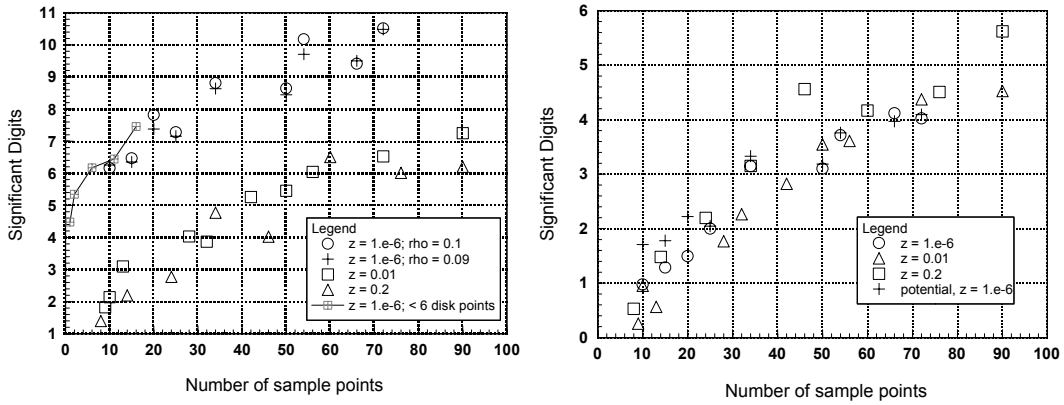

Fig. 2 – Convergence of components (a) normal gradient and (b) tangential gradient and potential.

References

[1] M. A. Khayat and D. R. Wilton, "Numerical Evaluation of Singular and Near-Singular Potential Integrals," *IEEE Trans. Antennas Propagat*., vol. 53, no. 10, pp. 3180-3190, Oct. 2005.

[2] P. W. Fink, D. R. Wilton, and M. A. Khayat, "Issues and Methods Concerning the Evaluation of Hypersingular and Near-Hypersingular Integrals in BEM Formulations", *Proc. ICEAA*, pp. 861-864, Torino, Italy, 2005.

[3] M. A. Khayat, D. R. Wilton, and P. W. Fink, "An Improved Transformation and Optimized Sampling Scheme for the Numerical Evaluation of Singular and Near-Singular Potentials", *Digest 2007 IEEE AP-S Int. Symp*., Honolulu (HI), June 10-15, submitted.

[4] P.W. Fink, D. R. Wilton, and M. Khayat, "Refinement of Methods for Evaluation of Near-Hypersingular Integrals in BEM Formulations", URSI National Radio Science Meeting, Albuquerque, N.M., 2006.

[5] M. G. Duffy, "Quadrature over a pyramid or cube of integrands with a singularity at a vertex," *SIAM J. Num. Anal.*, vol. 19, issue 6, pp. 1260–1262, 1982.